Journal of Iberian Geology
https://doi.org/10.1007/s41513-025-00320-x

RESEARCH PAPER

Analysis of the geothermal potential on the Iberian Peninsula using magnetic spectral method and comparison with other data in different tectonic domains

Alfonso Muñoz-Cemillán[1] · Alfonso Muñoz-Martín[1,2] · Antonio J. Olaiz[3] · Gerardo de Vicente[1]

Received: 14 December 2024 / Accepted: 2 October 2025

Abstract
Crustal geothermal data are of great interest for exploring energy resources, including hydrocarbons and medium- and high-enthalpy geothermal energy reservoirs. They are also of great interest in constraining the rheology of the Earth's crust and its potential to generate earthquakes. In this work, the Curie temperature depth (CTD) and other regional geothermal parameters (geothermal gradient and heat flow) on the Iberian Peninsula were calculated through spectral analysis of magnetic anomaly data that have been used to understand the regional thermal structure in other parts of the world. The obtained results include maps of the CTD, geothermal gradient, and heat flow that were compared with those obtained by previous authors using other methodologies, as well as with direct data included in the Global Heat Flow Data Base in four tectonic areas (Madrid Basin, Basque–Cantabrian Zone, Ebro Basin/Pyrenees, and the western margin of the Valencia Trough). This analysis revealed a positive correlation between the direct values obtained from wells and those calculated from magnetic data and discovered different geothermal crustal structures in the four areas analysed.

Keywords Curie temperature depth · Geothermal gradient · Heat flow · Magnetism · Spectral analysis · Iberian peninsula

Resumen
Los datos geotérmicos corticales son de gran interés para la exploración de recursos energéticos, incluidos los hidrocarburos y los yacimientos de energía geotérmica de media y alta entalpía. También son muy relevantes para determinar la reología de la corteza terrestre y su potencial generador de terremotos. En este trabajo se calcula la temperatura de profundidad de Curie (CTD, del inglés Curie temperature Depth) y otros parámetros geotérmicos regionales (gradiente geotérmico y flujo de calor) en la Península Ibérica mediante el análisis espectral de datos de anomalías magnéticas, un método utilizado para comprender la estructura térmica regional en otras partes del mundo. Los resultados obtenidos incluyen mapas de la CTD, el gradiente geotérmico y el flujo de calor, que se han comparado con los obtenidos por autores previos con otras metodologías, así como con los datos directos incluidos en la Base de Datos Global de Flujo de Calor en cuatro áreas tectónicas (Cuenca de Madrid, Zona Vasco-Cantábrica, Cuenca del Ebro/Pirineos y el margen occidental de la Surco de Valencia). Este análisis reveló, por un lado, una correlación positiva entre los valores directos obtenidos de sondeos y los calculados a partir de datos magnéticos y, por otro, mostró diferentes estructuras geotérmicas corticales en las cuatro áreas analizadas.

Palabras Clave Profundidad de temperatura de Curie · Gradiente geotérmico · Flujo de calor · Magnetismo · Análisis espectral · Península Ibérica

Extended author information available on the last page of the article

Published online: 20 October 2025

1 Introduction

Thermal data from the interior of the Earth's crust are essential for modern society. They support the exploration of energy resources, including hydrocarbons and medium- to high-enthalpy geothermal reservoirs (Stober & Bucher, 2021). Thermal data are also important for analysing the rheological behaviour of the crust and its seismogenic potential. However, obtaining thermal data from the interior of the Earth is a lengthy and costly process, as it is achieved by measuring temperature at various depths through two main methods:

A) Heat flow probes are used to study the seafloor. These short devices (usually less than 15 m) are driven into the most recent sediments, and the temperature is measured using sensors along their length. The main issue with this technique is that the data are very superficial and are restricted to recent sedimentary cover, making it challenging to extrapolate them to greater depths or areas without recent sedimentary records.
B) Through wells or research galleries, which are commonly used in exploring for hydrocarbons, mining, and, in some cases, hydrogeological research. In this approach, three main methods are used (Stober & Bucher, 2021): measuring the bottom hole temperature (BHT), using a thermal probe to record temperature variations along the well ("temperature log"), and measuring the temperature during production tests in hydrocarbon wells. The main challenge with these methods is often related to the high cost and logistical complexity of drilling and maintaining wells. Thermal disturbances during drilling and sound operations and water convection processes might also interfere with the accuracy of measurements and might bias geothermal gradient estimation.

These factors mean that the thermal values measured cannot be extrapolated to greater depths and/or over large areas without relative uncertainty.

1.1 Geophysical estimation of geothermal data at depth

Owing to the high cost of acquiring deep geothermal data, different authors have suggested the use of indirect data in geothermal resource exploration, including geochemical, geophysical, and geological methods (Glassley, 2015). Among these methods, the magnetic method stands out as the only one that directly provides information regarding temperature at a specific depth. This is because the magnetic behaviour of geological materials (rocks and minerals) is highly dependent on their temperature. Thus, any ferromagnetic material characterized by a high and positive magnetic susceptibility (k) transitions to paramagnetic behaviour (low and positive k) when it reaches the so-called "Curie temperature" (CT). In the crust, iron and titanium oxides (titanomagnetites) are the primary sources of magnetic anomalies (O'Reilly, 1976) and are particularly abundant in igneous and metamorphic rocks. The titanium fraction is low in acidic igneous and metamorphic rocks, and the Curie temperature can be approximately 580 °C (the value for magnetite). However, in some basic rocks, the titanium fraction may be significant, and in such cases, the CT may decrease to values close to 500 °C. Thus, the Curie temperature is generally assimilated to the value of magnetite (580 °C) for rocks with ferromagnetic minerals, namely, igneous and metamorphic rocks, that form the so-called "magnetic basement" and generate a strong magnetic signal. Owing to the absence of Fe–Mg minerals, sedimentary rocks exhibit paramagnetic behaviour and generate very weak magnetic signals (Fig. 1).

1.2 Calculation of the Curie temperature depth (CTD)

The principle of the Curie temperature depth (CTD) calculation is widely described in the literature: the CTD is located where the ferromagnetic behaviour of rocks changes to paramagnetic at depth, assuming that this depth corresponds to the 580 °C isotherm. The calculation of the "average" or regional geothermal gradient involves the assumption of a linear temperature response from the surface to the CTD. (Fig. 1).

Historically, magnetic data have been used to estimate the CTD through spectral analysis in the Fourier domain. Thus, the depth at which the magnetic signal is lost is calculated. On the basis of these spectral techniques, there are two main groups of calculation methods:

a) Methods that assume a random distribution of magnetic properties, as proposed by Bhattacharyya and Leu (1975), Okubo et al. (1985), and Tanaka et al. (1999). These methods typically involve analysing magnetic anomaly data by considering the statistical nature of the magnetic sources, enabling the estimation of the CTD on the basis of the depth of magnetic signal loss.
b) Methods that assume a fractal distribution of magnetization, as developed by Bouligand et al. (2009), Li et al. (2013), and Salem et al. (2014). These approaches consider the self-similar and scale-invariant nature of geological features and offer a more sophisticated subsurface model, which may improve the accuracy of CTD estimation by accounting for the complex distribution

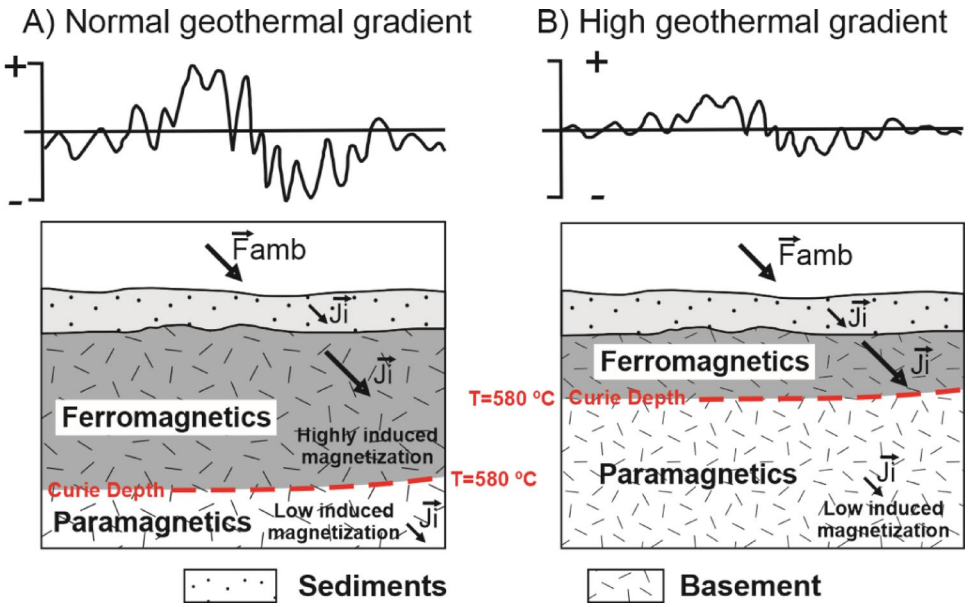

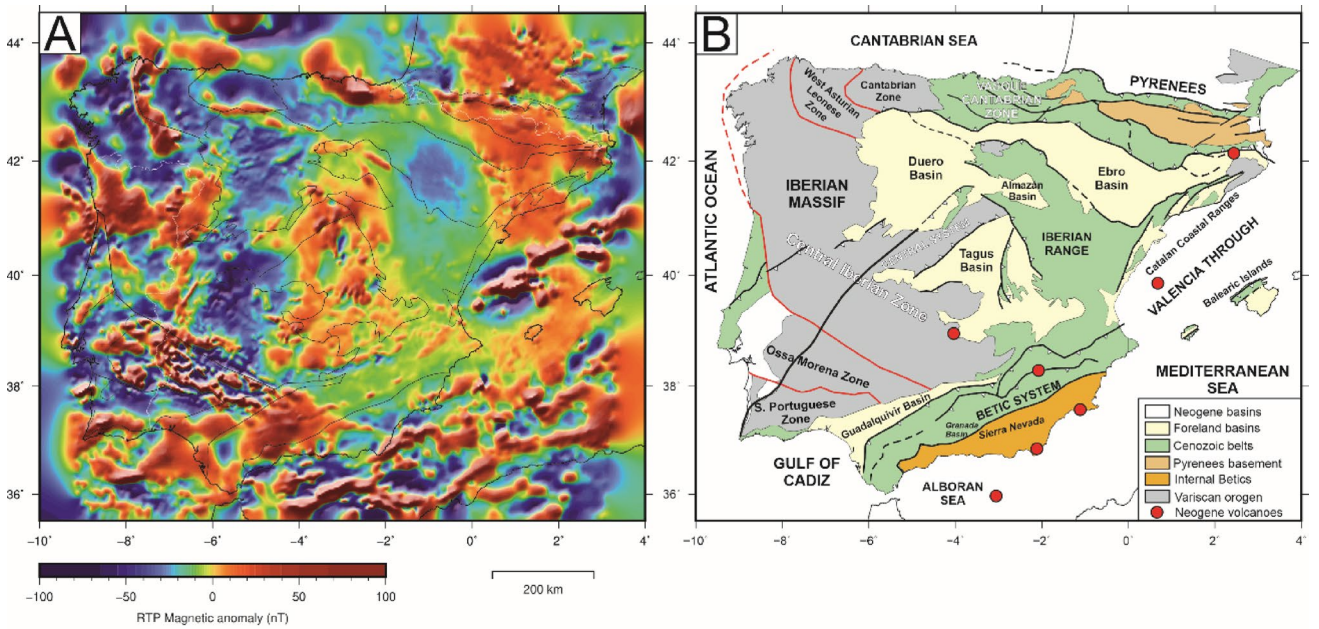

Fig. 1 Example of magnetic behaviour when an external magnetic field (Famb) acts to generate an induced magnetic field (Ji) in areas with **A** a low geothermal gradient (high CTD value) and **B** an area with a high geothermal gradient (low CTD value) (modified from Lillie, 1999)

Fig. 2 **A** Map of magnetic anomalies reduced to the pole on the Iberian Peninsula (data from Fletcher et al., 2011). **B** Tectonic zones of the Iberian Peninsula (modified from Vergés et al., 2019). The cartographic limits and units are used in the results and discussion sections

of magnetic sources. In some volcanic areas, the CTD method provides a deeper CTD than the fractal method does (e.g., Didas et al., 2022).

In this study, the Iberian Peninsula thermal structure was analysed by calculating the CTD and other geothermal parameters (geothermal gradient and heat flow) using spectral analysis of magnetic data. The results were compared with those of previous studies and with direct thermal data measured at depth in four tectonic settings. The Iberian Peninsula was chosen for this regional analysis because of the availability of high-quality magnetic data and its diverse geological settings, which provide an excellent opportunity for comparison with measured geothermal data (Fig. 2A). To achieve this primary objective, it was necessary to accomplish a series of partial objectives, which included the following: A) Calculation of the reduced-to-the-pole (RTP) magnetic anomaly and sensitivity analysis of the minimum grid size necessary for performing spectral parameter calculations. B) Creation of a regular sampling mesh centred every 50 km and the establishment of a set of 357 RTP magnetic anomaly grids for computing spectral calculations on

the Iberian Peninsula. C) Determination of the CTD using the method of Tanaka et al. (1999) for the set of 357 grids of RTP magnetic anomalies. D) Estimation of the geothermal gradient and heat flow on the Iberian Peninsula by integrating the calculated geothermal gradient values with the Moho depth map (Díaz et al., 2016). E) Comparison of thermal data (geothermal gradient and heat flow) with previous results obtained by other authors and with direct data from boreholes in four different geological settings.

Finally, the applicability of the methodology and limitations in identifying areas of potential interest for geothermal exploration are discussed.

2 Data description

The application of these methods for estimating CTDs requires high-quality magnetic data with appropriate spatial coverage. Fortunately, on the Iberian Peninsula, various magnetic databases with high-quality data are accessible (Ardizone et al., 1989; Dyment et al., 2020). However, for this study, we used high-resolution data, licenced by Repsol. The magnetic database was compiled and leveled by Getech, which processed terrestrial and marine data acquired by Repsol and the Spanish Geological Survey (IGME-CSIC) (Fletcher et al., 2011). The database includes data from various aeromagnetic flights and marine surveys that cover the entire surface of the Iberian Peninsula and its adjacent areas. To achieve a continuous grid, Getech filled the survey gaps using data from EMAG2 (Maus et al., 2009). The data are referenced to a flight altitude of 1 km, and the resolution of the final grid is 0.01°, which is approximately 1000 m at the mean Iberian latitude. Finally, reduced-to-pole (RTP) magnetic anomalies were calculated for the inclination, declination, and reference date, and these values were resampled to a grid interval of 2000 m using kriging with a linear variogram. The resulting grid formed the basis for estimating the depths of the magnetic sources and CTD (Fig. 2A).

Depth data from the Mohorovičić (Moho) discontinuity are essential for estimating heat flow because they depend on conductivity (K) and radiogenic production (A), which are very different in the crust and mantle (see explanation in Sect. 3). To calculate heat flow, we used the database compiled by Díaz et al. (2016; Fig. 3A), which includes data from deep controlled-source seismic profiles and passive seismic data from the Topo-Iberia Project (Gallart et al., 2015). Integrating both datasets creates a regional Moho surface that includes the Iberian Peninsula, its continental margins, and northern Morocco (Fig. 3A).

We used data from the Global Heat Flow Database (GHFDB) to calibrate the thermal results obtained from the magnetic data. This public database includes worldwide thermal data updated from 1938 to 2023 (Fuchs et al., 2023) and was established in 1963 by the International Heat Flow Commission (IHFC). This commission compiles global thermal data from 1939, encompassing geothermal gradient and heat flow data. From this extensive database, 1,264 data points located within the study area were analysed

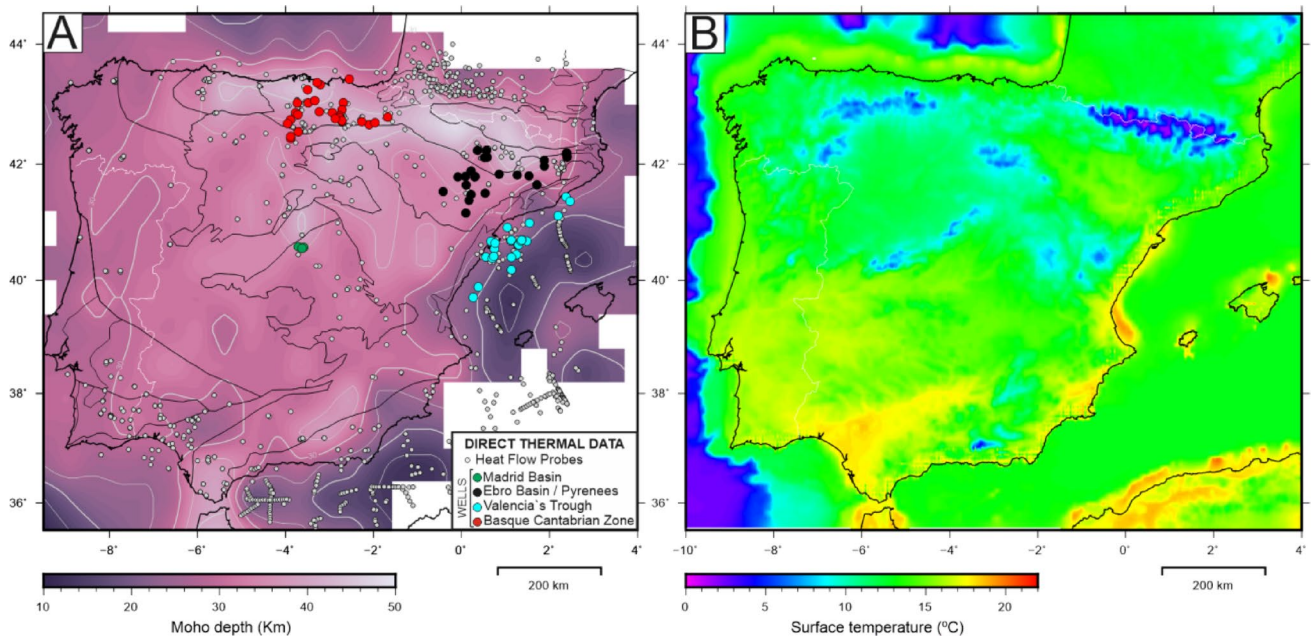

Fig. 3 **A** Map of the depth of the Moho discontinuity, derived from the dataset compiled by Díaz et al. (2016). The circles represent the GHFDB data (Fuchs et al., 2023), whereas the coloured circles denote the boreholes used for comparison with the parameters calculated from the magnetic data. **B** Map of the average land surface and seafloor temperatures (°C) obtained from the Copernicus Climate Change Service database of the European Union (https://climate.copernicus.eu/)

(Fig. 3A). In this study, only the highest-quality data were used; data obtained at depths of less than 300 m were discarded because of their lower representativeness of deep thermal data. After filtering, four study areas were defined to assess the results in different geological contexts, encompassing 83 deep wells with thermal data. The four selected areas are the Madrid Basin, the Basque–Cantabrian Zone, the Ebro Basin/Pyrenees, and the continental margin of the Valencia Trough (Fig. 3A). All these data correspond to hydrocarbon exploration and production wells.

Surface temperature data are necessary to estimate the geothermal gradient accurately (see methodology below). In this study, terrestrial surface temperature data from the Iberian Peninsula and ocean floor temperature data from the Copernicus Programme (Climate Change Service of the European Union) were used. To obtain the final map, terrestrial surface temperature data for 2012 were used, and the annual average was calculated. Similarly, the same calculation was performed for the sea floor temperature. Finally, all the data were integrated into a single regular grid with a 2000 m cell size (Fig. 3B).

3 Methodology

The basics of CTD estimation are presented below, followed by an explanation of the workflow used to calculate the derived thermal variables (geothermal gradient and heat flow).

3.1 Calculation of Curie temperature depth (CTD)

Two fundamental methods exist for estimating the CTD from magnetic data. On the one hand, one method utilizes the shape of the magnetic anomaly (Bhattacharyya & Leu, 1975). On the other hand, one method analyses the statistical properties of magnetic anomaly patterns (Spector and Grant, 1970). Both methods provide a relationship between the spectrum of magnetic anomalies and the depth of a magnetic source.

The method proposed by Tanaka et al. (1999) is based on Spector and Grant (1970) and assumes that the top boundary (Z_t) and the centroid (Z_0) of a magnetic source are calculated from the power spectrum of the magnetic anomalies. These two values can be used to estimate the basal depth of a magnetic source (Z_b). The method assumes that the layer extends in all horizontal directions for the analysed grid, that the depth of the top boundary of a magnetic source is small compared to its horizontal scale and that the magnetization M(x,y) is a random function of x and y. Under these conditions, Blakely (1996) reported that the power density spectra of the total field anomaly ($\Phi_{\Delta T}$) can be simplified by assuming radial symmetry.

$$\begin{aligned}\Phi_{\Delta T}\left(k_x,k_y\right) &= \Phi_M\left(k_x,k_y\right) \times F\left(k_x,k_y\right)\\ &= 4\pi^2 C_m^2 \left|\theta_m\right|^2 \left|\theta_f\right|^2 \left(1-e^{-2|k|\left(Z_b-Z_t\right)}\right)^2\end{aligned} \tag{1}$$

where Φ_M is the power density spectrum of the magnetization, C_m is a proportionality constant, and m and f are factors for the magnetization direction and the geomagnetic field direction, respectively.

This equation can be simplified by considering that all terms are radially symmetric, except $|\Theta_m|^2$ and $|\Theta_f|^2$, and that the radial averages of Θ_m and Θ_f are constants. Thus, the radial average of $\Phi_{\Delta T}$ can be defined as follows:

$$\Phi_{\Delta T}\left(|k|\right) = Ae^{-|k|Z_t}1-e^{-|k|\left(Z_b-Z_t\right)2} \tag{2}$$

where A is a constant. For wavelengths greater than twice the thickness of the layer, Eq. (1) becomes:

$$\ln\Phi_{\Delta T}\left(|k|\right)^{1/2} = \ln B - |k|\,Z_t \tag{3}$$

where B is a constant, and we can calculate the top of the magnetic source (Z_t) on the basis of the slope of the magnetic anomaly spectrum.

Moreover, Equation [3] for long wavelengths can be rewritten as follows:

$$\begin{aligned}\Phi_{\Delta T}\left(|k|\right)^{1/2} &= Ce^{-|k|Z_0}e^{-|k|(-d)}\\ &\quad - e^{-|k|(d)} \sim Ce^{-|k|Z_0}2\mathrm{d}\ \ |k|\end{aligned} \tag{4}$$

where C is a constant and 2d is the thickness of the magnetic source. Finally, this equation can be expressed as follows:

$$\ln\left\{\left[\Phi_{\Delta T}\left(|k|\right)^{1/2}\right]\Big/|k|\right\} = \ln D - |k|\,Z_0 \tag{5}$$

where D is a constant and Z_0 is the magnetic centroid depth. In this way, the upper boundary of the magnetic source (Zt) and the centroid (Z_0) can be estimated by fitting a straight line to the high- and low-wavenumber segments of the radial spectrum, respectively. Finally, the basal depth of the magnetic source (Z_b or Curie temperature depth, CTD) is as follows:

$$Z_b = \mathrm{CTD} = 2Z_0 - Z_t \tag{6}$$

An example of a power spectrum from magnetic anomaly data, along with the fitting of two segments of the power spectrum slope, is shown in Fig. 4. The segment with a higher wavenumber (K) corresponds to the upper boundary (magnetic basement top, Z_t). In contrast, the segment with a lower value of K corresponds to the centroid depth (Z_0) of a horizontally extending magnetic layer. The basal depth of the magnetic signal (Z_b) corresponds to the CTD and reflects an average depth in the grid used for the calculation. The calculation of the radial spectra of magnetic anomalies, as well as the slopes of the high and low segments of the spectrum, was performed using Oasis Montaj software and its 2D frequency domain data processing module (Fig. 4B).

Since the centroid value is calculated in the low segment of the spectrum (longer wavelengths), a sufficiently large grid size is necessary to capture the lowest frequencies and observe the spectrum's decline. Only when the spectrum shape is well defined in its low segment can its slope be reliably calculated (and consequently, the value of Z_b). The minimum size of the magnetic anomaly grid is discussed further in the sensitivity analysis.

3.2 Geothermal gradient calculation

Once the average CTD is calculated for each grid, an average geothermal gradient for the centre of each grid can be estimated. To calculate this gradient more realistically, average surface temperature or ocean floor temperature values were used as the surface temperature (Fig. 3B). In this way, the following expression defines the geothermal gradient.

$$GG = \left(\frac{T_C - Tsup}{Z_b}\right) \tag{7}$$

where T_C is the Curie temperature (580 °C), Tsup is the surface (or ocean floor) temperature, and Z_b is the Curie temperature depth (CTD) calculated using Equation [6].

3.3 Heat flow calculations

For heat flow (Q_0) calculations, we followed the methodology proposed by Andrés et al. (2018), which considers whether the CTD is located above or below the Moho discontinuity (Fig. 5). To achieve this, it is necessary to compare the CTD values with the depth of the Moho (Díaz et al., 2016), resulting in two cases depending on whether the CTD is above or below the Moho surface.

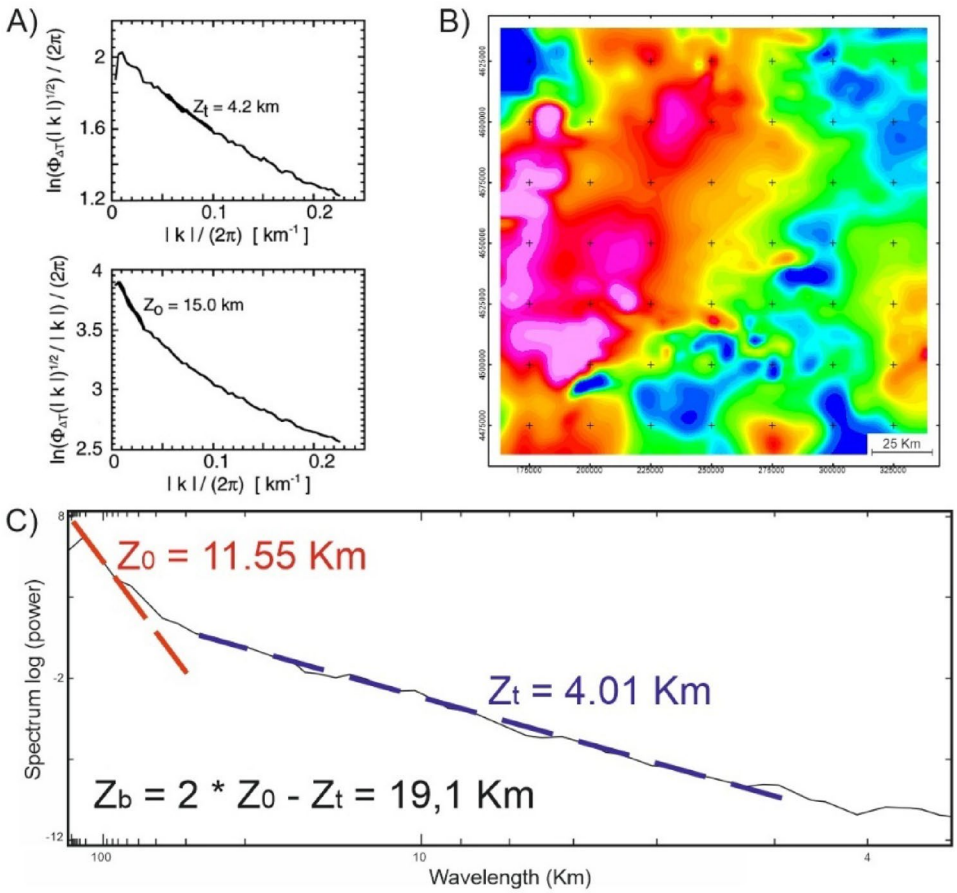

Fig. 4 **A** Example of the estimation of Z_0 and Z_t values from the slope of the radial magnetic anomaly spectrum (modified from Tanaka et al., 1999). **B** One of the 357 RTP magnetic anomaly grids (175 km grid size) used to calculate geothermal parameters. **C** Radial energy spectrum and calculation of Z_0, Z_t, and Z_b for this grid (see text for explanation)

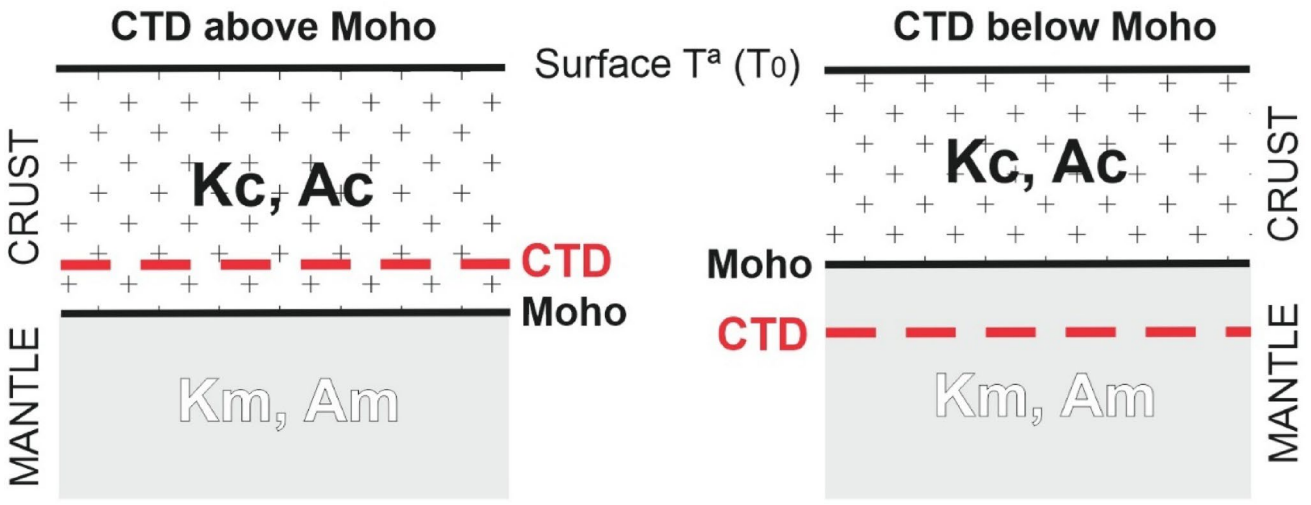

Fig. 5 Two possible cases for the calculation of geothermal flow. Left: The CTD is located above the Moho, and only the values of conductivity and crustal heat production (Kc and Ac, respectively) are assumed. Right: The CTD is situated below the Moho, and both the conductivity and heat production values of the crust (Kc and Ac, respectively) and the mantle (km, Am) are used (modified from Andrés et al., 2018)

A) For CTD values located above the Moho discontinuity, it is assumed that both heat production (Ac) and conductivity (Kc) correspond to the average values of the Earth's crust. Therefore, the radiogenic heat production value used (Ac) is 1 μW/m^3, and the chosen crustal thermal conductivity value (Kc) is 2.2 W/m·°C. In this case, the heat flow (Q0) is calculated using the following expression:

$$Q_O = \frac{A_c \cdot CTD}{2} + \frac{(T_C - T_0) \cdot K_c}{CTD} \quad (8)$$

where A_C is the crustal heat production (μW/m^3), CTD is the Curie temperature depth (m), T_C is the Curie temperature (580 °C), T_0 is the surface temperature (or ocean floor temperature, °C), and K_C is the crustal thermal conductivity (2.2 W/m·°C).

B) For CTDs located below the Moho, mantle productivity (A_m) and thermal conductivity (K_m) values of 0 μW/m^3 and 2.7 W/m·°C, respectively, are assumed, in addition to the crustal values above the Moho. The expression used for the calculation of heat flow in this case is as follows:

$$Q_O = \frac{\left[(T_C - T_0) + A \cdot Z_m \cdot (CTD - Z_m)/K_m + A \cdot Z_m^2/2 \cdot K_c\right]}{\left[\frac{Z_m}{K_c} + (CTD - Z_m)/K_m\right]} \quad (9)$$

where A_C is the crustal heat production (1 μW/m^3), A_m is the mantle heat production (0 μW/m^3), K_C is the crustal conductivity (2.2 W/m·°C), K_m is the mantle conductivity (2.7 W/m·°C), T_0 is the surface temperature, T_C is the Curie temperature (580 °C), CTD is the Curie temperature depth (m), and Z_m is the Moho depth (m).

3.4 Grid size sensitivity analysis

Given the importance of the minimum magnetic grid size analysed to estimate the centroid depth, a sensitivity analysis of this parameter was developed. A set of square RTP magnetic anomaly grids with different side lengths was created to achieve this (Fig. 6A). The centre of all these grids was located in the centre–western part of the Iberian Peninsula to ensure a sufficient richness of high- and low-frequency magnetic signals. For this analysis, Z_t (top of the magnetic source), Z_0 (centroid depth), and CTD were calculated starting from a grid with a side length of 50 km and progressively increasing in size until reaching a maximum size of 300 km (Fig. 6A). Table 1 and Fig. 6 present the results of the CTD values and geothermal gradient-calculated grid size. The results indicate that smaller grid sizes (<125 km) yield geothermal gradient results that are out of range and unstable. Beyond this threshold, the values of the CTD and the geothermal gradient stabilize, albeit with some variation due to the increased surface area analysed. A grid size of 175 km was selected to ensure sufficient coverage for both the aerial and marine data. To obtain a regional distribution of CTD values, a regular mesh of 357 sampling points spaced 50 km apart was designed (Fig. 7), and at each sampling point, a 175 km-long RTP magnetic anomaly square grid was defined. The central point of each grid was used to

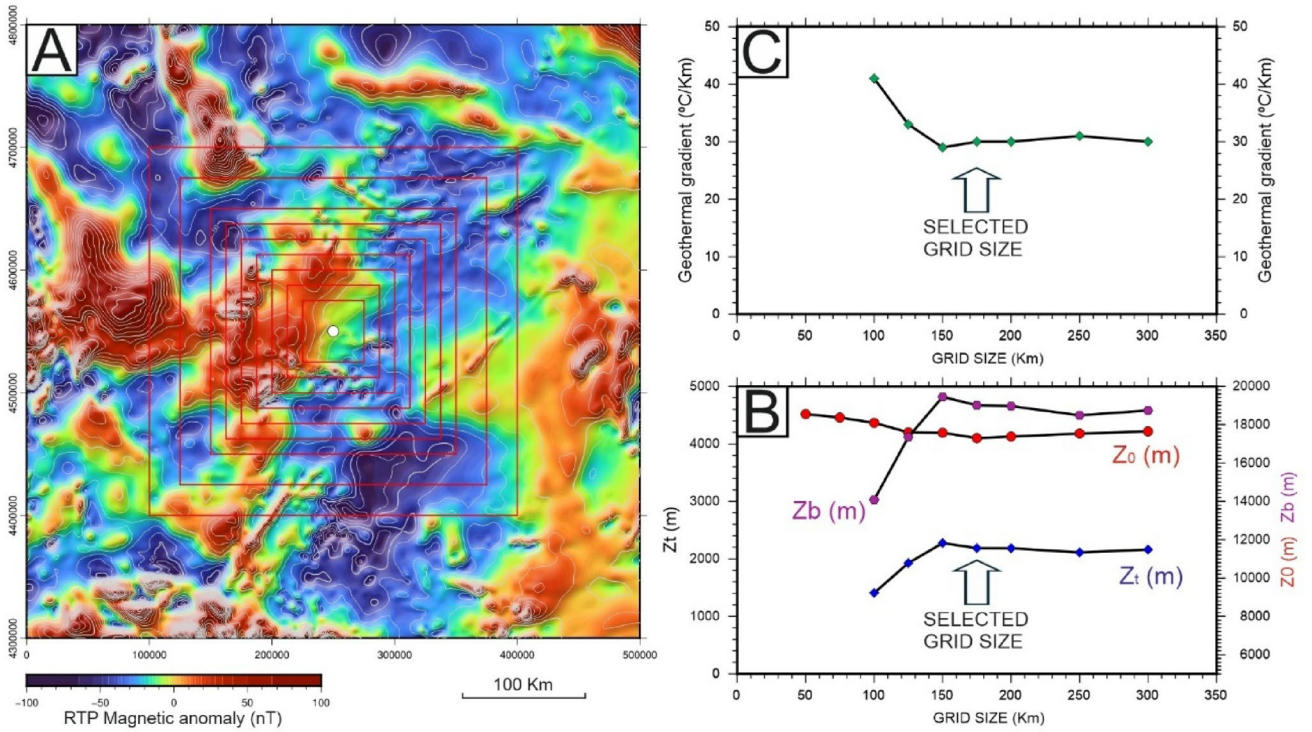

Fig. 6 **A** RTP magnetic anomaly grids used for the sensitivity analysis of the minimum grid size to be used in the spectral calculation of geothermal parameters (ranging from 50 to 300 km in length). **B** Representation of the Z_t, Z_0, and Z_b (Curie temperature depth) and **C** geothermal gradient versus different grid sizes. The selected grid size for spectral analysis is shown (175 km)

Table 1 Results obtained from the sensitivity analysis of the grid size of the RTP magnetic anomaly using spectral analysis (the grids used and results are shown in Fig. 6A)

Grid size (Km)	Zt (m)	Z0 (m)	CTD (m)	GG (°C/Km)
50	4518	–	–	–
75	4458	–	–	–
100	4366	9222	13,078	44,35
125	4199	10,778	16,357	35,46
150	4192	11,822	18,452	31,43
175	4099	11,556	18,013	32,20
200	4127	11,549	17,971	32,27
250	4178	11,334	17,490	33,16
300	4215	11,480	17,745	32,69

Zt, top of the magnetic basement; Z0, centroid depth; CTD, Curie temperature depth; and GG, geothermal gradient

calculate the thermal parameters, resulting in a grid overlap of more than one-third of the grid size.

4 Results

The following sections present the maps calculated for the CTD, geothermal gradient, and heat flow derived from magnetic data using the previously described methodology. The boundaries of the tectonic zones proposed by Vergés et al. (2019) were superimposed to aid in the analysis and discussion, as shown in Fig. 2B. Finally, the calculated parameter values were compared with the measured values from the well data.

4.1 Curie temperature depth (CTD) map

As previously indicated, the CTD map illustrates the depth at which the magnetic signal disappears. Consequently, high CTD values imply areas with a lower geothermal gradient and typically correspond to cold and rigid continental crust regions. Conversely, areas with low CTD values indicate a high geothermal gradient associated with thinned crust or areas that have undergone more recent tectonic–magmatic processes. The CTD distribution map is shown in Fig. 8, with calculated values ranging from 25.2 km on the Iberian Massif (Central System) to an absolute minimum of 11.2 km on the southeastern Iberian Peninsula. The average CTD value for this dataset is 17.98 km. This suggests that, for the continental crust, the map depicts variations in thermal parameters that impact the upper and middle crust. Despite its low spatial resolution (lateral variations > 50 km), the map shows a correlation with first-order geological units: areas with deeper CTD values mainly correspond to the Iberian Massif, particularly the Central Iberian Zone, which represents the part of Iberia that was not subjected to rifting processes during the Mesozoic. In contrast, shallower CTD values are

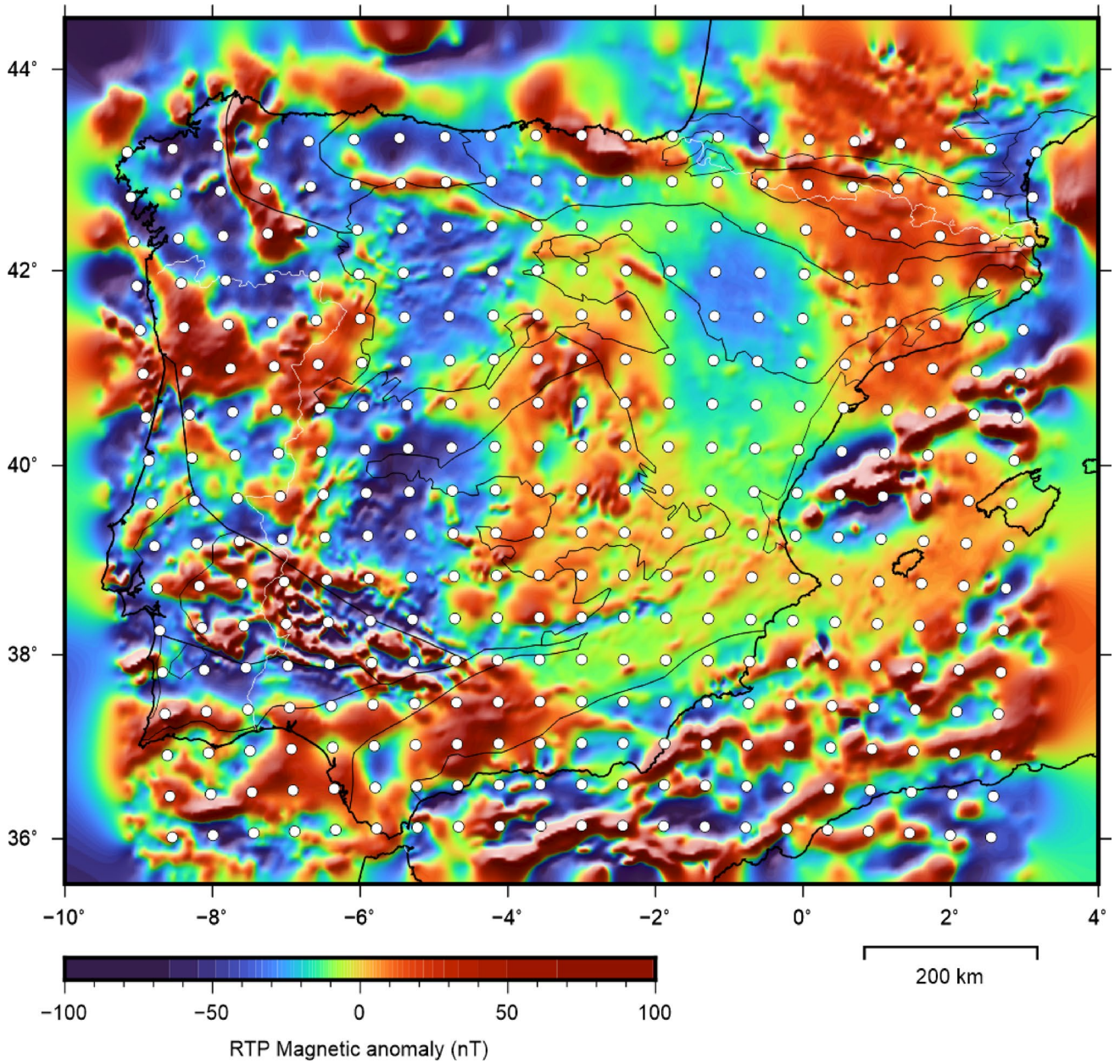

Fig. 7 Map showing 357 sample points (regularly spaced every 50 km), where spectral analysis of RTP magnetic anomalies (Fletcher et al., 2011) and geothermal parameter calculations were performed

present in Atlantic areas (Gulf of Cádiz) and, mainly, in the Mediterranean Sea (western margin of the Valencia Trough and the Alboran Sea). The shallowest CTD values are found within the continental zone in the Basque–Cantabrian Zone, southeastern Iberian Peninsula, Iberian Range, and Catalan coastal ranges. The situation appears more complex in the Pyrenees and the northern Iberian Peninsula, with low CTD values in the Basque–Cantabrian Zone and the central sector of the Pyrenean Axial Zone, as well as in the northern and southern regions of Galicia (NW Iberian Peninsula). This alternation of highs and lows in the CTD also appears to the south, affecting the Betic Cordillera and the southern edge of the Iberian Massif, with a more pronounced variation than that observed in the Pyrenees. This pattern could be related to more recent tectonic activity in these southern regions.

Despite its regional nature, the map allows the inference of several first-order discontinuities (crustal faults) that are likely to impact the upper to middle crust. Among these faults, the contact between the southern limit of the Central System and the Cenozoic Tagus Basin is notable and involves a vertical displacement of several kilometres in the

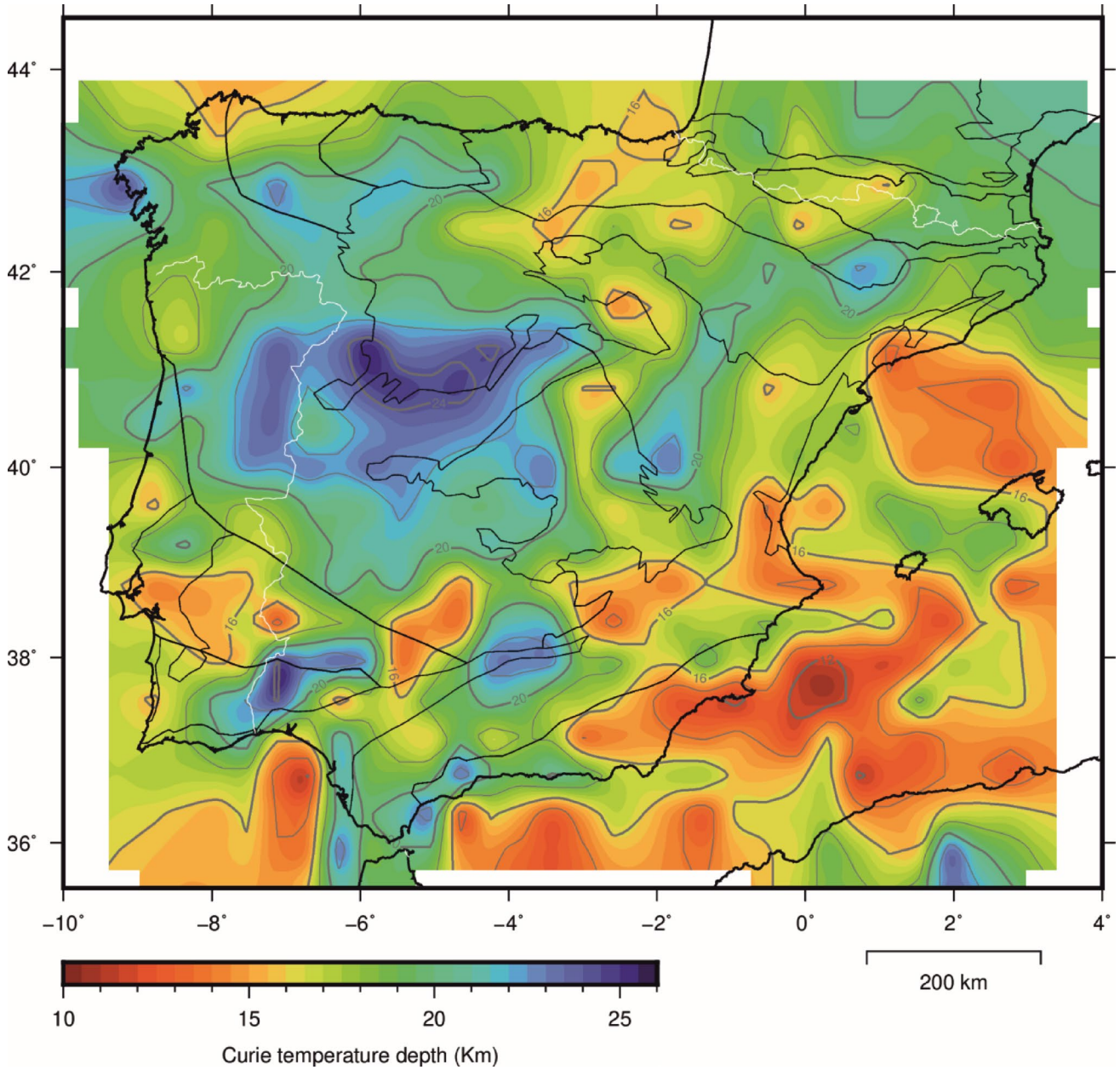

Fig. 8 Curie temperature depth (CTD) map derived from spectral analysis of magnetic data

ferromagnetic basement (De Vicente and Muñoz Martín, 2013) and the NNE–SSW faults on the northwestern Iberian Peninsula (De Vicente et al., 2011).

In the Iberian Range, there is a minimum parallel to the Mediterranean coast, and to the west, there is a parallel maximum, which is unrelated to the Variscan part of the crust. The maximum ends against the neighbouring minima, forming an arc. This structural arrangement could explain the large-scale isostatic uplift of the central part of the Iberian Range, with the consequent incision of the river network (Casas-Sainz and De Vicente, 2009).

4.2 Geothermal gradient map

The average geothermal gradient (Fig. 9) in the study area is 33.2 °C/km, ranging from 23 °C/km in the Central System to an absolute maximum of 52 °C/km in the Mediterranean, southeastern Iberian Peninsula. The distribution of geothermal gradient values closely follows the pattern observed in the CTD map. Minimum geothermal gradient values are on the Iberian Massif (especially in the Central System). Low values are also found in southeastern Galicia (NW Iberia) and some sectors of the Betic Cordillera. Conversely, the maximum geothermal gradient values are located in the

Mediterranean Sea, southern and eastern Iberian Peninsula. The maximum geothermal gradient values for the continental zone are in the Basque–Cantabrian Zone and the E and SE areas of the Iberian Peninsula. Additionally, a maximum gradient appears in the Ossa Morena Zone within the Iberian Massif.

4.3 Heat flow map

The distribution of heat flow values calculated under the assumption of a homogeneous crust and heat transfer by conductivity (Eqs. (7) and (8)) is shown in Fig. 10. The zones of highest thermal flow (reaching up to 122 mW/m^2) are primarily associated with the Mediterranean region, particularly the extended continental crust between the Iberian Peninsula and the Balearic Islands and the oceanic crust between Algeria and the southeastern Peninsula. In this area, the Balearic Islands correlate well with a minimum in thermal flow, likely because of less crustal extension and a relatively thicker crust, typically resulting in lower heat flow than in more extensively thinned regions.

The maximum heat flow values in southeastern zones align with recent volcanic activity in SE Iberia (volcanic areas of Calatrava, Murcia–Almería, Columbretes, and Alborán Island). These areas benefit from the geothermal effects of underlying magmatic activity, contributing to

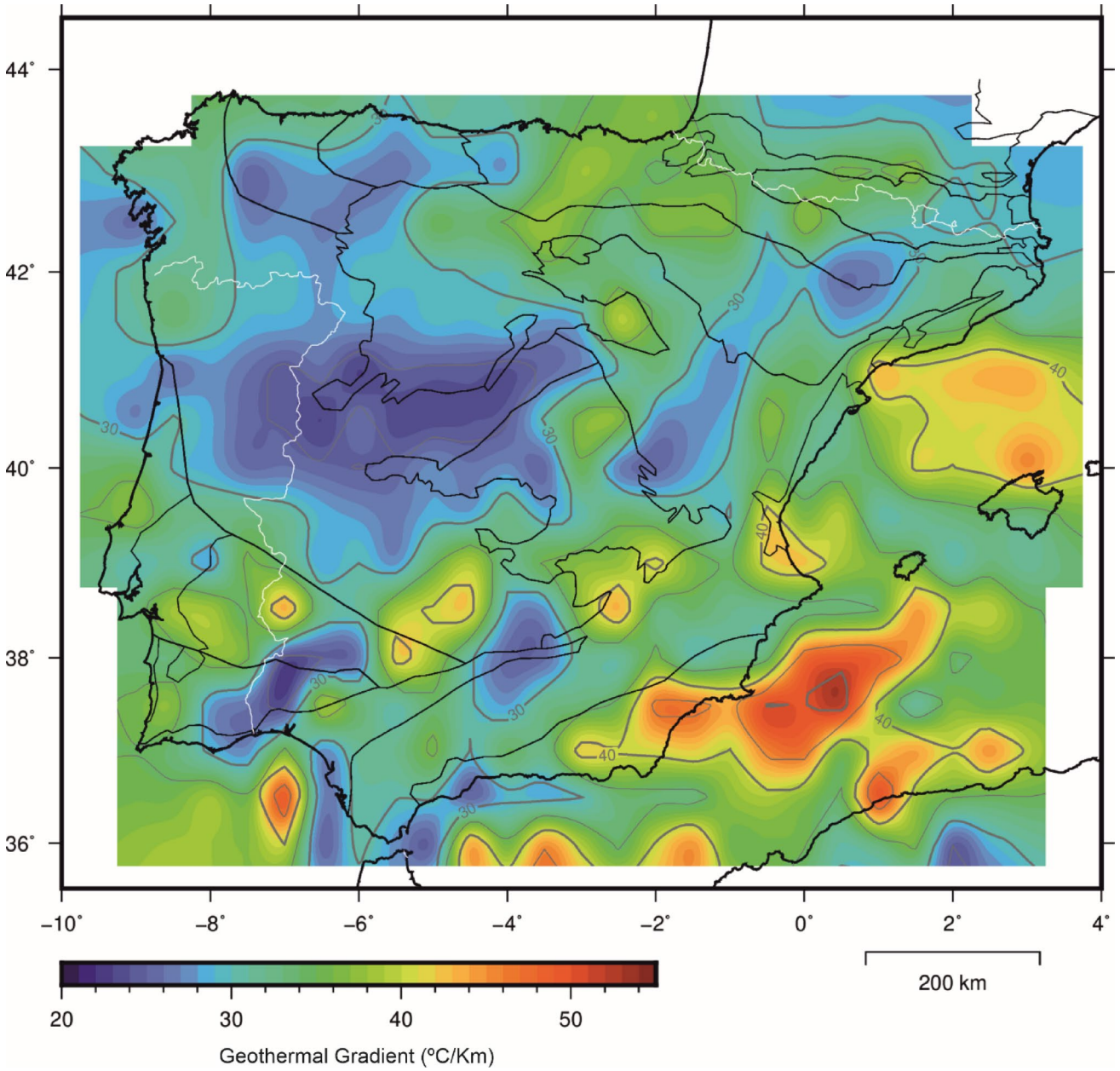

Fig. 9 Geothermal gradient map (°C/km) calculated from spectral analysis of magnetic data

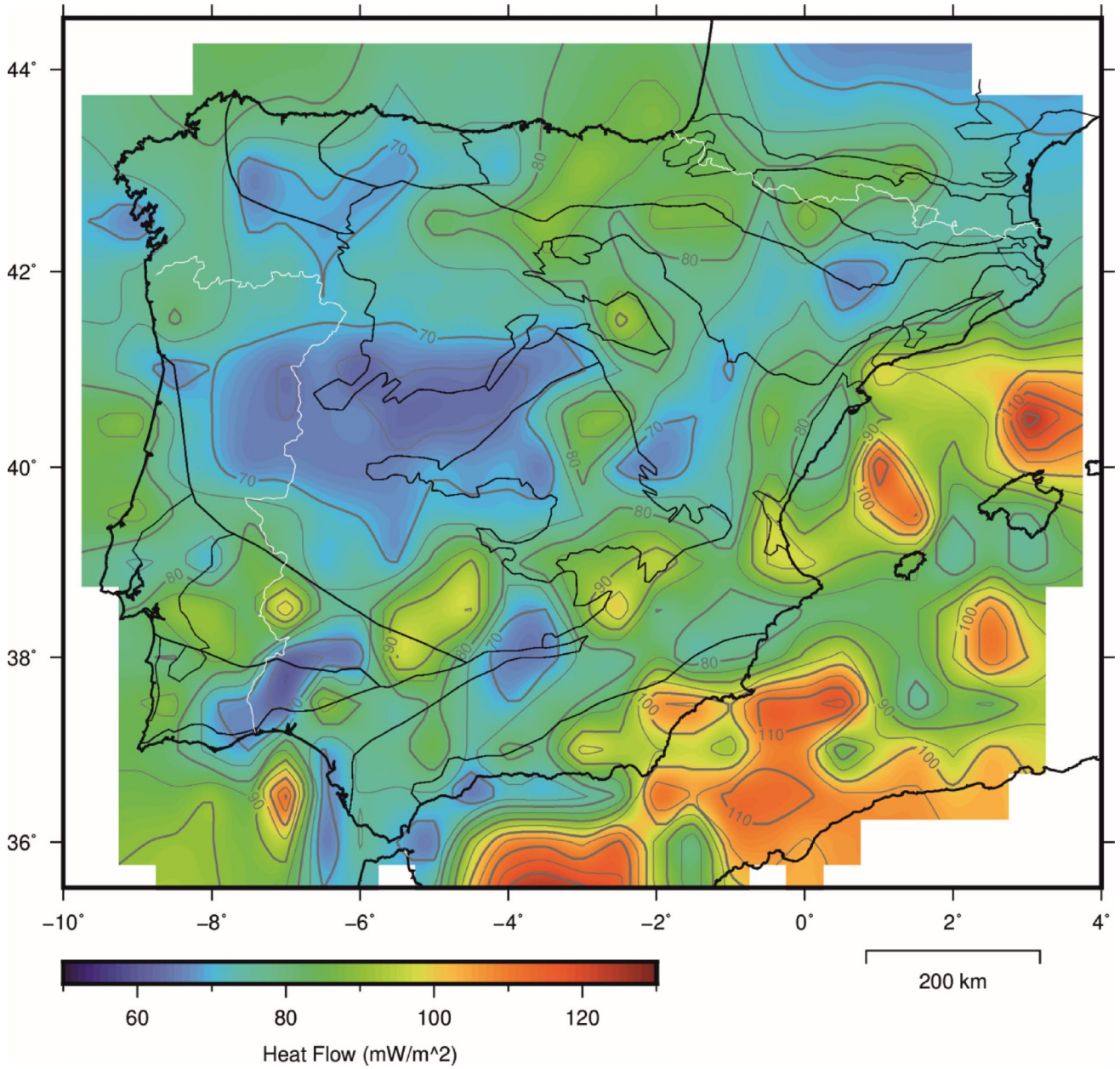

Fig. 10 Heat flow map (mW/m^2) calculated from spectral analysis of magnetic data

increased heat flow. On the other hand, the Olot volcanic area (NE Iberia) does not appear to have maximum heat flow values on the thermal flow map. In the peninsula interior, the maximum heat flow values are in the Basque–Cantabrian Zone, the axial zone of the Pyrenean Range, and some sectors of the Betic Cordillera and its northwestern front. Lower heat flow values (62 mW/m^2) are primarily located on the Iberian Massif, notably in the Central Iberian Zone, the Central System, and the area southeast of Galicia. Other places with low heat flow values include specific sectors of the Betic Cordillera, the Iberian Range, and the southwestern Peninsula, encompassing the Ossa Morena and South Portuguese Zones.

Given the correlation of the map with the geology of the Iberian Peninsula, it is possible to identify some less apparent anomalies. High thermal flow values are present in the Cenozoic basins of Almazán and northern parts of the Duero and Ebro Basins. These maxima seem to border the eastern limit of the Iberian Massif. Within the Betic Cordillera, the Sierra Nevada area is highlighted by an east–west maximum in the Granada Basin that ends towards the west. Generally, this range is characterized by abrupt changes in

heat flow values (short wavelengths), which also occur with variations in active stresses (De Vicente et al., 2008).

5 Discussion

The method used in this study enables the calculation of mean CTD values for an average surface area (175 * 175 km), assuming a random distribution of magnetic materials, and, for heat flow, a purely conductive behaviour and a homogeneous crust. Owing to the last assumption, the observed variations in heat flow (Fig. 9) may also be influenced by other factors, such as lithological heterogeneity, especially in the continental crust. In this sense, such maps do not consider crust with high heat-producing capacity (e.g., crust with a high content of granites rich in radiogenic minerals). Nevertheless, these results are consistent on a regional scale, and the values are within the range of those of previous studies based on various methodologies.

5.1 Comparison of results obtained by previous authors

In this work, it is helpful to compare the data calculated from magnetic data with those of medium- and high-enthalpy resources because of their greater extent and regional characteristics. In this sense, our results were compared with maps of medium- and high-enthalpy geothermal resources published by IDAE/IGME (Guzmán et al., 2011). The coincident zones of high potential between the results of this work and those proposed by Guzmán et al. (2011) for medium- and high-enthalpy geothermal energy are the Basque–Cantabrian Zone, the Madrid Basin, the area indicated on the southeastern Iberian Peninsula, and the area near the Valencia Trough (Catalan Coastal Ranges). These authors identified additional minor regional geothermal resources, predominantly in areas with springs or thermal waters (e.g., in Galicia and the other regions in the Centro Iberian Zone). There is no evident correlation between these observations and the CTD data or the geothermal gradient estimated from magnetic data for these cases. The underlying cause may be related to the heat transfer mechanism in these locations, which is associated with the upwelling of deep fluids along structural discontinuities affecting the upper crust. These fractures likely act as genuine conductive zones that focus heat transfer to the surface predominantly through advection rather than conduction. This heat transfer mechanism was not considered in this study because of the regional scale of work and the assumptions made for heat flow calculations, which assume that heat transfer occurs exclusively through conduction. Another reason might be that the geothermal resources in these areas are representative of very local anomalies, whereas the estimations from magnetic spectra are smoothed out by the data windowing procedure, providing only regional indications (Didas et al., 2022).

Other authors (Andrés et al., 2018) have calculated geothermal parameters on the Iberian Peninsula using different magnetic data with an alternative sample grid and employing a different methodology through Pycurious software (Mather and Delhaye, 2019), which assumes a fractal distribution of magnetic elements in the crust. The results obtained are very similar in terms of values and distribution to those obtained in this work, demonstrating the robustness of the spectral analysis of magnetic data in the regional calculation of thermal parameters.

Table 2 A summary of the well data used for the four analysed zones is shown in Fig. 3A

Selected zones	N	Max GG (°C/Km)	Min GG (°C/Km)	Min heat flow (mW/m^2	Max heat flow (mW/m^2
Madrid Basin	3	40	31	70	86
Vasco-Cantabrian zone	27	37	22	69	113
Ebro Basin/ Pyrenees	22	41	22	65	113
Valencia's Through	31	46	28	59	122

N, number of wells; Max GG, maximum geothermal gradient value (°C/km); Min GG, minimum geothermal gradient value (°C/km); Min heat flow: minimum heat flow value (mW/m^2); and Max heat flow: maximum heat flow value (mW/m^2)

5.2 Comparison with thermal well data

Comparisons were made between the results of this work and the direct geothermal depth data obtained from the Global Heat Flow Database (GHFDB) in four areas of the Iberian Peninsula (Fig. 3A, Table 2). The regions were selected on the basis of geological criteria (different tectonic contexts) and the availability of sufficient wells with reliable data. Despite the limited number of deep wells in the Madrid Basin (only three), they were included in the analysis because of the reliability of the data obtained from these wells. Notably, some of these wells were drilled explicitly for geothermal exploration (San Sebastian and Tres Cantos), and the temperature values were carefully corrected. To analyse the two types of data, the gradient and geothermal flow values calculated in this work and those measured in wells are represented in X/Y scatter plots. For this purpose, the calculated grid values derived from the magnetic data were extracted for each well. On the X-axis, the direct

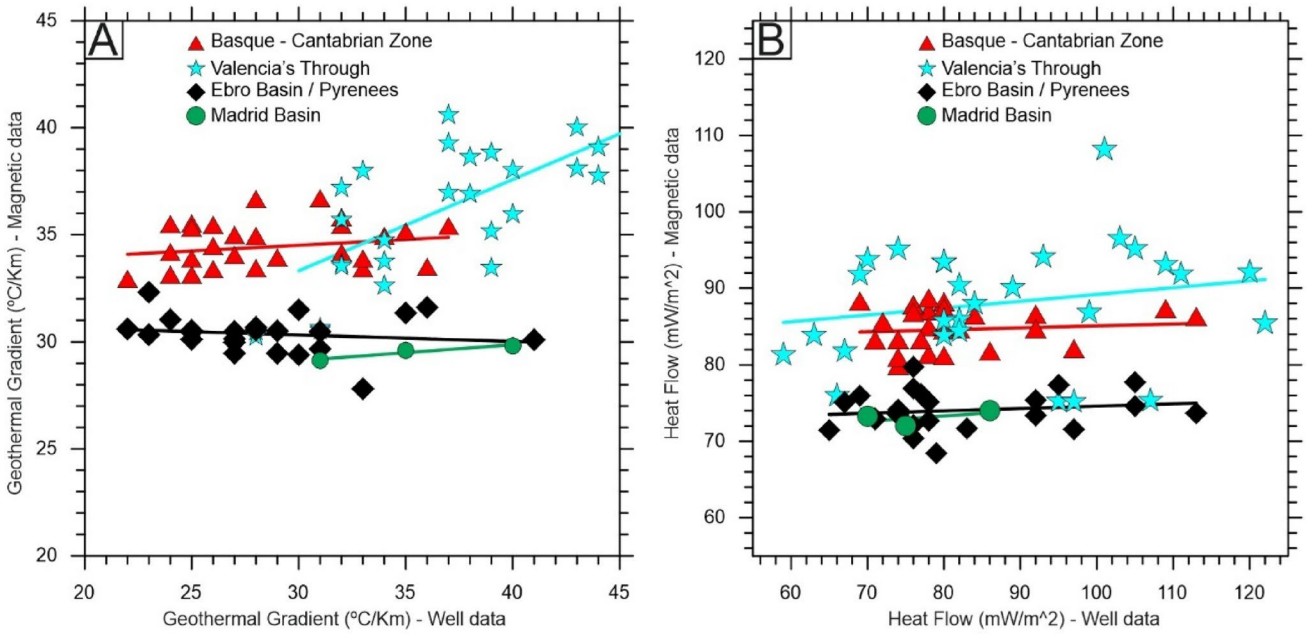

Fig. 11 Scatter plots showing geothermal parameter data calculated from the spectral analysis of magnetic data and well data. **A** Geothermal gradient values (°C/km). **B** Geothermal heat flow (mW/m.^{2})

geothermal data (°C/km) are represented, and on the Y-axis, the geothermal data obtained from the magnetic data are displayed (Fig. 11).

The geothermal gradient data plotted in Fig. 11A show, despite the scatter, a similar trend for the four analysed areas. This trend is linear with a positive slope, and the gradient values measured in wells are somewhat more significant than those estimated from the magnetic data. This could be because the values calculated from magnetic data are "regional" average values that may be considered "minimum" gradient values. The slope of the trend line is similar to the lower gradient values in the Madrid and Ebro/Pyrenees Basins. The values from the Basque–Cantabrian Zone show higher geothermal gradient values in both data types and a slope similar to those of the previous two areas. The western margin of the Valencia Trough has higher geothermal gradient values, with more similar values between the measured and calculated data but with greater dispersion. Despite the dispersion, the results allow us to deduce a higher value of the geothermal gradient in the Basque–Cantabrian Zone, western margin of the Valencia Trough, and somewhat lower and very similar gradients in the Madrid Basin and in the Ebro/Pyrenees Basin. The magnetic data results facilitate the identification of areas with elevated geothermal gradient values, as measured in wells. It is plausible that the higher values observed in wells may be attributed to the influence of additional heat transfer mechanisms beyond conduction and the presence of local geological heterogeneities that are not discernible through the methodology employed in this study.

The distributions of heat flow values (mW/m^2) measured in boreholes and those estimated from magnetic data are shown in Fig. 11B. Despite the scatter, a behaviour similar to that observed with geothermal gradient data is evident, with a linear trend fit and positive slopes of low magnitude. This graph also indicates that the heat flow data measured in boreholes are always somewhat higher than the thermal data calculated from magnetic data. In the case of heat flow, all slopes are similar, which is not the case for the geothermal gradient in the Valencia Trough. Although the data from the Madrid Basin, Ebro/Pyrenees Basin, and Basque–Cantabrian Zone are less scattered, the data from the continental margin of the Valencia Trough are more scattered, with heat flow values exceeding 100 mW/m^2 both in wells and from magnetic data. The maximum flow values are on the margin of the Valencia Trough and the Basque–Cantabrian Zone, and they are lower and very similar in the Ebro Basin/Pyrenees and the Madrid Basin. The heat flow values from wells are significantly greater than those derived from magnetic data, with greater differences than in the case of geothermal gradients. This difference is likely related to two aspects: a) the different scales between the calculations derived from magnetic data and direct observations (as also occurs in the case of the geothermal gradient); and b) the data obtained from wells reflecting additional heat transfer mechanisms that are not considered in the study methodology, such as heat transfer associated with the circulation of hot fluids from deep origins through conductive zones (advective mechanisms). The results indicate that, as with the geothermal gradient values, magnetic data enable the calculation

of geothermal flow on a regional scale, which smooths the well-measured values.

6 Conclusions

The values obtained for all geothermal parameters, which are based on the spectral analysis of magnetic data by Tanaka et al. (1999), fall within the range of previous studies that have assumed a different distribution of ferromagnetic minerals, employed alternative calculation methods, or utilized distinct data sources. These results validate the efficacy of spectral techniques applied to magnetic data for thermal characterization of the crust on a regional scale, which is beneficial for identifying regions with diverse exploratory potential for geothermal reservoirs. Furthermore, these data are highly valuable for establishing boundary conditions for other geological studies, including those related to crustal rheology.

The results obtained allow for the identification of zones that are strongly correlated with the main geological units of the Iberian Peninsula. The CTD ranges from 11 km in the southeastern part of the Iberian Peninsula to 25 km on the Iberian Massif (Central System). In comparison, the calculated geothermal gradient values range from 23 to 51 °C/km (23 to 41 °C/km for the continental area). The calculated heat flow values range from 60 mW/m^2 on the Iberian Massif (Central System) to 122 mW/m^2 on the southeastern Iberian Peninsula. In the continental part, the maximum thermal flow values are located in the Basque–Cantabrian Zone, sectors of the Betic Cordillera, Pyrenees, and coastal Catalan ranges.

The areas with the lowest geothermal gradient and heat flow are in regions of old and cold crust (Iberian Massif) that were not subjected to Mesozoic rifting processes. In contrast, the areas exhibiting the highest gradient and geothermal flow values are in regions where the crust has been subjected to more recent tectonic processes, including crustal extension and volcanism. These regions include the Basque–Cantabrian Zone, specific sectors of the Betic Cordillera, and the western margin of the Valencia Trough.

The gradient and geothermal flow values calculated from the magnetic data correlate with the well-measured values and exhibit distinct behaviours in the four geological zones analysed. The calculated geothermal parameters typically exhibit lower values than those observed in wells, which is likely related to the following factors:

a) The values calculated from magnetic data are determined as an average of 175 km per side for grid sizes, giving them a regional character (smoother).
b) The heat flow calculations from magnetic data assume a conductive behaviour without accounting for other thermal transfer mechanisms (convection/advection).
c) The radiogenic production and conductivity values employed for the crust and mantle have remained constant throughout the Iberian Peninsula. Despite this simplification, the maps illustrate variations that reflect the compositional heterogeneity of the crust above the CTD in crusts of similar ages and thicknesses.

The geothermal results from magnetic data should be complemented on a smaller scale with detailed geological characterization, considering local heterogeneities and other conductive/advective thermal transport mechanisms.

Acknowledgements This work was funded by a Master's grant from Repsol, S.A. and by CARESOIL (PR37/24 TEC-2024/ECO-69) and GEOMARHIS projects (GEOMARHIS, PID2022-138360NB-I00). The authors would like to extend their gratitude to Repsol and Getech for providing the magnetic data for this work. The GMT software system from Wessel et al. (2019) was invaluable for drawing maps and figures.

Declarations

Conflict of interest On behalf of all the authors, the corresponding author states that there are no conflicts of interest.

References

Andrés, J., Marzán, I., Ayarza, P., Martí, D., Palomeras, I., Torné, M., & Carbonell, R. (2018). Curie point depth of the Iberian Peninsula and surrounding margins. A thermal and tectonic perspective of its evolution. *Journal of Geophysical Research: Solid Earth, 123*(3), 2049–2068.

Ardizone, J., Mezcua, J. Y., & Socias, I. (1989). Mapa aeromagnético de España peninsular Instituto Geográfico Nacional, Madrid. *MOPU, 1*, 1.

Bhattacharyya, B. K., & Leu, L. K. (1975). Analysis of magnetic anomalies over Yellowstone National Park: Mapping curie point isothermal surface for geothermal reconnaissance. *Journal of Geophysical Research, 80*(32), 4461–4465.

Blakely, R. J. (1996). *Potential theory in gravity and magnetic applications*. Cambridge University Press.

Bouligand, C., Glen, J. M. G., & Blakely, R. J. (2009). Mapping Curie temperature depth in the western United States with a fractal model for crustal magnetization. *Journal of Geophysical Research, 114*, B11104. https://doi.org/10.1029/2009JB006494

Casas-Sainz, A. M., & De Vicente, G. (2009). On the tectonic origin of Iberian topography. *Tectonophysics, 474*(1–2), 214–235.

De Vicente, G., Cloetingh, S. A. P. L., Van Wees, J. D., & Cunha, P. P. (2011). Tectonic classification of Cenozoic Iberian foreland basins. *Tectonophysics, 502*(1–2), 38–61.

De Vicente, G., & Muñoz-Martín, A. (2013). The Madrid basin and the Central System: A tectonostratigraphic analysis from 2D seismic lines. *Tectonophysics, 602*, 259–285.

Diaz, J., Gallart, J., & Carbonell, R. (2016). Moho topography beneath the Iberian-Western Mediterranean region mapped from controlled-source and natural seismicity surveys. *Tectonophysics, 692*, 74–85.

Didas, M. M., Armadillo, E., Hersir, G. P., Cumming, W., & Rizzello, D. (2022). Regional thermal anomalies derived from magnetic spectral analysis and 3D gravity inversion: Implications for potential geothermal sites in Tanzania. *Geothermics, 103*, 102431.

Dyment, J., Choi, Y., Lesur, V., Garcia-Reyes, A., Catalan, M., Ishihara, T., ... & Hamoudi, M. (2020). The World Digital Magnetic Anomaly Map: version 2.1. *In EGU General Assembly Conference Abstracts*, p. 22098.

Fletcher, K. M. U., Fairhead, J. D., Salem, A., Lei, K., Ayala, C., & Cabanillas, P. L. M. (2011). Building a higher resolution magnetic database for Europe for resource evaluation. *First Break*

Fuchs, S., Norden, B., Neumann, F., Kaul, N., Tanaka, A., Kukkonen, I. T., & Verdoya, M. (2023). Quality-assurance of heat-flow data: The new structure and evaluation scheme of the IHFC Global Heat Flow Database. *Tectonophysics, 863*, 229976.

Gallart, J., Azor, A., Fernández, M., & Pulgar, J. A. (2015). Iberia geodynamics: An integrative approach from the Topo-Iberia framework. *Tectonophysics, 663*, 1–4.

Glassley, W.E. (2015). *Geothermal Energy: Renewable Energy and the Environment*, Second Edition (2nd ed.). CRC Press.

Guzmán, J. S., López, L. S., & Robles, L. O. (2011). *Evaluación del potencial de energía geotérmica*. Estudio Técnico PER 2011–2020. Jaume Margarit i Roset, IDAE, Madrid

Lafuente, P., Arlegui, L. E., Liesa, C. L., & Simón, J. L. (2011). Paleoseismological analysis of an intraplate extensional structure: The Concud fault (Iberian Chain, eastern Spain). *International Journal of Earth Sciences, 100*, 1713–1732.

Li, C. F., Wang, J., Lin, J., & Wang, T. (2013). Thermal evolution of the North Atlantic lithosphere: New constraints from magnetic anomaly inversion with a fractal magnetization model. *Geochemistry, Geophysics, Geosystems, 14*(12), 5078–5510.

Lillie, R. J. (1999). *Whole earth geophysics*. Prentice Hall.

Mather, B., & Delhaye, R. (2019). Pycurious: A Python module for computing the Curie depth from the magnetic anomaly. *Journal of Open Source Software, 4*(39), 1544.

Maus, S., et al. (2009). EMAG2: A 2-arc-minute resolution Earth Magnetic Anomaly Grid compiled from satellite, airborne and marine magnetic measurements. *Geochemistry, Geophysics, Geosystems, 10*, Q08005.

O'Reilly, W. (1976). Magnetic minerals in the crust of the Earth. *Reports on Progress in Physics, 39*(9), 857.

Okubo, Y., Graf, R. J., Hansen, R. O., Ogawa, K., & Tsu, H. (1985). Curie point depths of the island of Kyushu and surrounding areas, Japan. *Geophysics, 50*(3), 481–494.

Salem, A., Green, C., Ravat, D., Singh, K. H., East, P., Fairhead, J. D., & Biegert, E. (2014). Depth to Curie temperature across the central red sea from magnetic data using the de-fractal method. *Tectonophysics, 624*, 75–86.

Spector, A., & Grant, F. S. (1970). Statistical models for interpreting aeromagnetic data. *Geophysics, 35*(2), 293–302.

Stober, I., & Bucher, K. (2021). Uses of Geothermal Energy. *Geothermal Energy: From Theoretical Models to Exploration and Development* (pp. 43–79). Springer International Publishing.

Tanaka, A., Okubo, Y., & Matsubayashi, O. (1999). Curie point depth based on spectrum analysis of the magnetic anomaly data in East and Southeast Asia. *Tectonophysics, 306*(3–4), 461–470.

Vergés, J., Kullberg, J. C., Casas-Sainz, A., de Vicente, G., Duarte, L. V., Fernàndez, M., & Vegas, R. (2019). *An introduction to the Alpine cycle in Iberia* (pp. 1–14). The geology of Iberia: A geodynamic approach: Volume 3: The Alpine cycle.

De Vicente, G. D., Cloetingh, S. A. P. L., Muñoz-Martín, A., Olaiz, A., Stich, D., Vegas, R., ... & Fernández-Lozano, J. (2008). Inversion of moment tensor focal mechanisms for active stresses around the microcontinent Iberia: Tectonic implications. *Tectonics*

Wessel, P., Luis, J. F., Uieda, L., Scharroo, R., Wobbe, F., Smith, W. H. F., & Tian, D. (2019). The generic mapping tools version 6. *Geochemistry, Geophysics, Geosystems, 20*(11), 5556–5564. https://doi.org/10.1029/2019GC008515

Authors and Affiliations

Alfonso Muñoz-Cemillán[1] · Alfonso Muñoz-Martín[1,2] · Antonio J. Olaiz[3] · Gerardo de Vicente[1]

✉ Alfonso Muñoz-Martín
amunoz@ucm.es

Alfonso Muñoz-Cemillán
alfomu01@ucm.es

Antonio J. Olaiz
antoniojose.olaiz@repsol.com

Gerardo de Vicente
gdv@geo.ucm.es

[1] Applied Tectonophysics Group, GEODESPALFacultad de Ciencias Geológicas, Universidad Complutense de Madrid, Madrid, Spain

[2] Instituto de Geociencias IGEO (CSIC-UCM), Madrid, Spain

[3] Repsol E&P, C/Méndez Álvaro 44, 28045 Madrid, Spain